


Crystal structure of ractopamine hydrochloride, C₁₈H₂₄NO₃ClColin W. Scherry,¹ Nicholas C. Boaz,¹ James A. Kaduk ^{1,2,a)} Anja Dosen ³ and Thomas N. Blanton ³¹North Central College, 131 S. Loomis St., Naperville, IL 60540, USA²Illinois Institute of Technology, 3101 S. Dearborn St., Chicago IL 60616, USA³ICDD, 12 Campus Blvd., Newtown Square, PA, 19073-3273, USA

(Received 8 November 2023; accepted 7 February 2024)

The crystal structure of ractopamine hydrochloride has been solved and refined using synchrotron X-ray powder diffraction data, and optimized using density functional theory techniques. Ractopamine hydrochloride crystallizes in space group *Pbca* (#61) with $a = 38.5871(49)$, $b = 10.7691(3)$, $c = 8.4003(2)$ Å, $V = 3490.75(41)$ Å³, and $Z = 8$. The ractopamine cation contains two chiral centers, and the sample consists of a mixture of the S,S/R,R/S,R and R,S forms. Models for the two diastereomers S,S and S,R were refined, and yielded equivalent residuals, but the S,R form is significantly lower in energy. The crystal structure consists of layers of molecules parallel to the *bc*-plane. In each structure one of the H atoms on the protonated N atom acts as a donor in a strong discrete N–H⋯Cl hydrogen bond. Hydroxyl groups act as donors in O–H⋯Cl and O–H⋯O hydrogen bonds. Both the classical and C–H⋯Cl and C–H⋯O hydrogen bonds differ between the forms, helping to explain the large microstrain observed for the sample. The powder pattern has been submitted to ICDD® for inclusion in the Powder Diffraction File™ (PDF®).

© The Author(s), 2024. Published by Cambridge University Press on behalf of International Centre for Diffraction Data. This is an Open Access article, distributed under the terms of the Creative Commons Attribution licence (<http://creativecommons.org/licenses/by/4.0/>), which permits unrestricted re-use, distribution and reproduction, provided the original article is properly cited.

[doi:10.1017/S0885715624000095]

Keywords: ractopamine hydrochloride, Paylean®, crystal structure, Rietveld refinement, density functional theory

I. INTRODUCTION

Ractopamine is an animal feed additive used to promote leanness and increase food conversion efficiency in farmed animals. It is the active ingredient in products marketed in the US as Paylean for swine, Optaflexx for cattle, and Topmax for turkeys. It was developed by Elanco Animal Health, a division of Eli Lilly and Company. As of 2014, the use of ractopamine was banned in 160 countries (Pacelle, 2014), including the European Union, China, and Russia, while 27 other countries, such as Japan, the United States, South Korea, and New Zealand have deemed meat from livestock fed with ractopamine to be safe for human consumption. The systematic name (CAS Registry Number 90274-24-1) is 4-(1-hydroxy-2-((4-(4-hydroxyphenyl)butan-2-yl)amino)ethyl)phenol hydrochloride. A two-dimensional molecular diagram of ractopamine as downloaded from PubChem (Kim et al., 2023) is shown in Figure 1.

Ractopamine has two chiral centers, one the so-called “OH-site” and the other the “Me-site” (Gunnar et al., 2009). Commercial ractopamine hydrochloride is a mixture of all four isomers. The R,R (OH,Me) isomer is known to be the most potent (Ricke et al., 1999; Mills et al., 2003a, 2003b). The hydrochloride salt of the R,R isomer is known as butopamine hydrochloride (Gunnar et al., 2009). R,R-ractopamine

is not chirally stable, but epimerizes over a period of days. In contrast, R,R/S,R-ractopamine is an isomerically stable mixture (Gunnar et al., 2009). We are unaware of any published X-ray powder diffraction data for ractopamine hydrochloride.

This work was carried out as part of a project (Kaduk et al., 2014) to determine the crystal structures of large-volume commercial pharmaceuticals, and include high-quality powder diffraction data for them in the Powder Diffraction File (Gates-Rector and Blanton, 2019).

II. EXPERIMENTAL

Ractopamine hydrochloride was a commercial reagent, purchased from USP (Batch R066T0), and was used as-received. The white powder was packed into a 1.5-mm diameter Kapton capillary, and rotated during the measurement at ~50 Hz. The powder pattern was measured at 295 K at a beam line 11-BM (Antao et al., 2008; Lee et al., 2008; Wang et al., 2008) of the Advanced Photon Source at Argonne National Laboratory using a wavelength of 0.458208(2) Å from 0.5° to 50° 2θ with a step size of 0.001° and a counting time of 0.1 s/step. The high-resolution powder diffraction data were collected using twelve silicon crystal analyzers that allow for high angular resolution, high precision, and accurate peak positions. A mixture of silicon (NIST SRM 640c) and alumina (NIST SRM 676a) standards (ratio Al₂O₃:Si = 2:1 by weight) was used to calibrate the instrument and refine the monochromatic wavelength used in the experiment.

^{a)} Author to whom correspondence should be addressed. Electronic mail: kaduk@polycrystallography.com



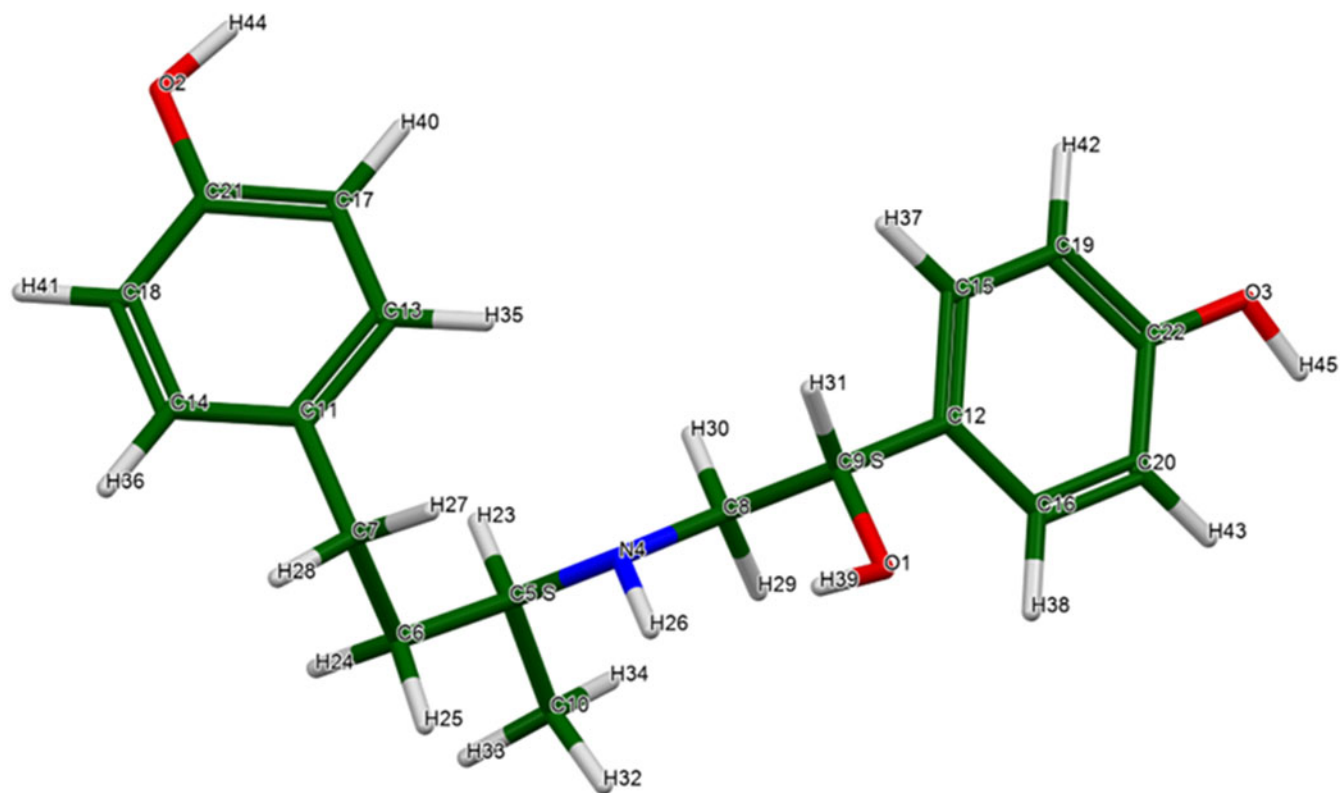


Figure 1. The structure of the neutral ractopamine molecule, as downloaded from PubChem (Kim et al., 2023), showing the S,S configuration. Image generated using Mercury (Macrae et al., 2020).

The synchrotron diffraction peaks are observed to be broad, and do not extend to high angles (Figure 2). After a number of unsuccessful attempts using several programs, the pattern was indexed using DICVOL06 (Louër and Boulfif, 2007) as incorporated into EXPO2014 (Altomare et al., 2013) on a high-quality primitive orthorhombic unit cell with $a = 38.49578$, $b = 10.75221$, $c = 8.39423$ Å, $V = 3474.49$ Å³, and $Z = 8$. A reduced cell search in the Cambridge Structural Database (Groom et al., 2016) with the chemistry C, H, Cl, N, and O only yielded six hits, but no ractopamine derivatives.

Several programs indicated different space groups, but both JANA2006 (Petricek et al., 2014) and DASH (David et al., 2006) suggested that *Pbca* was most probable. This suggestion was confirmed by a successful solution and refinement of the structure.

The ractopamine molecule (S,S) was downloaded from PubChem (Kim et al., 2023) as Conformer3D_CID_56052.sdf. It was converted to a *.mol2 file using Mercury (Macrae et al., 2020), and to a Fenske-Hall Z-matrix using OpenBabel (O'Boyle et al., 2011). The crystal structure was solved using

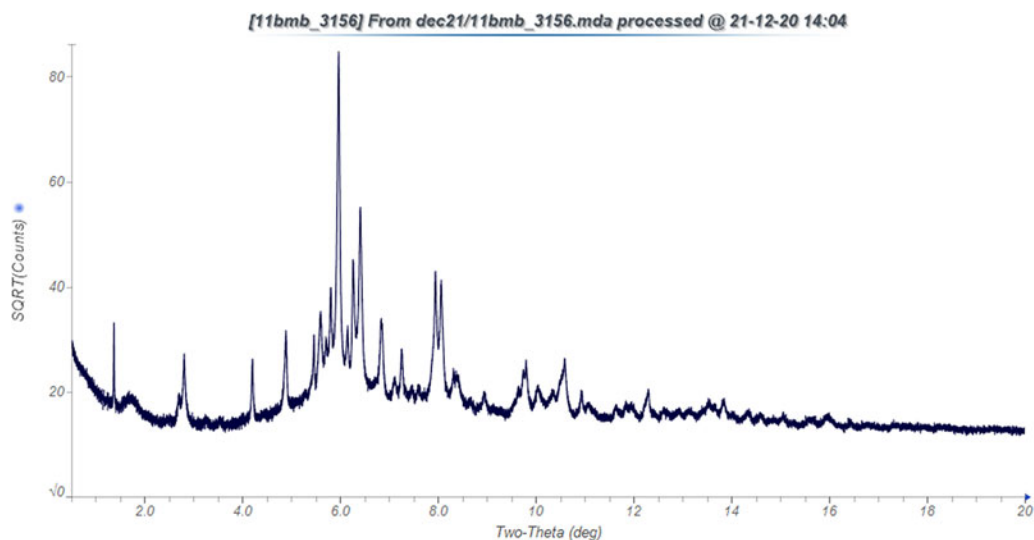


Figure 2. The synchrotron powder pattern of ractopamine hydrochloride, measured at 11-BM at APS using a wavelength of 0.458208 Å. Image generated using JADE Pro (MDI, 2023).

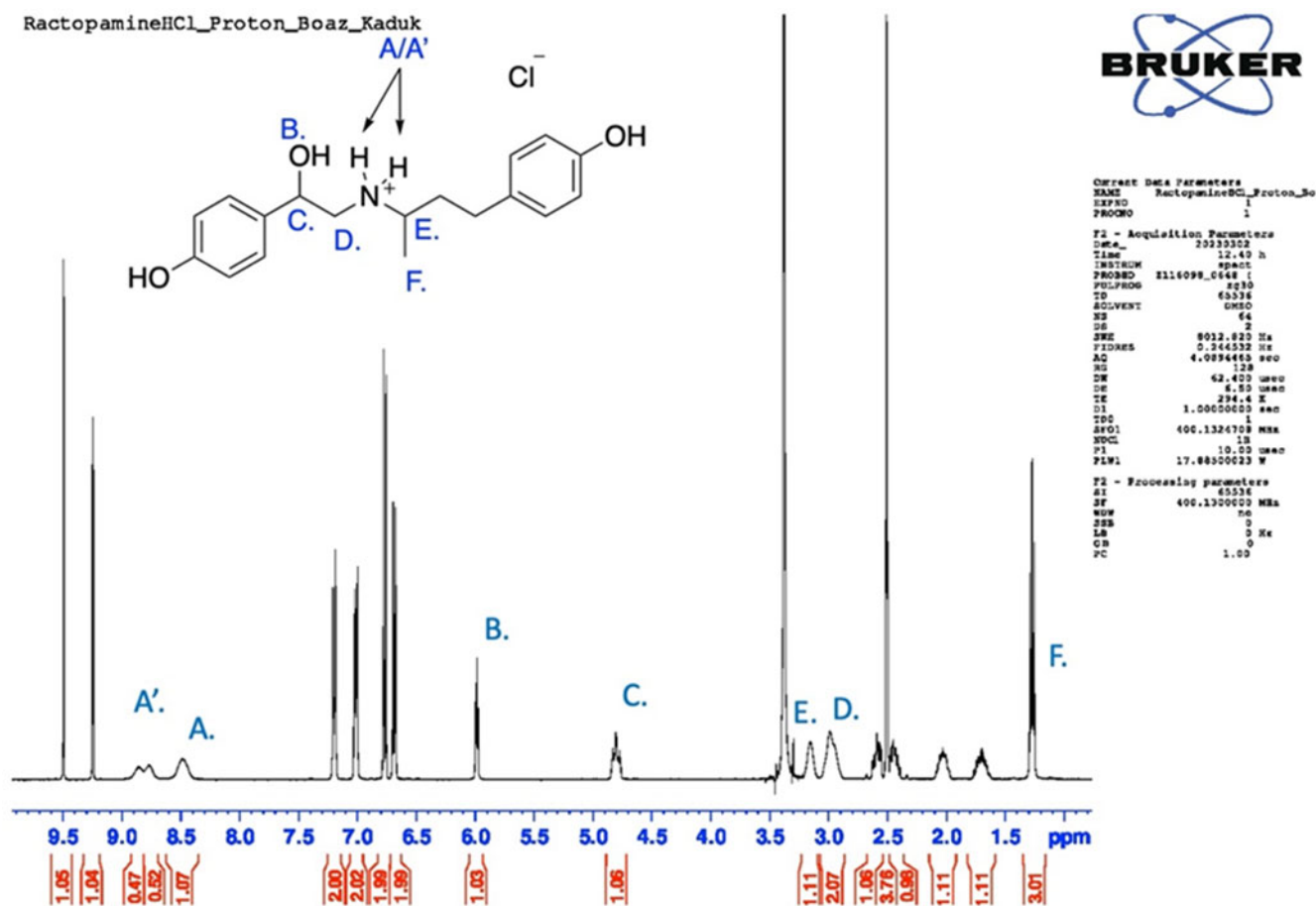


Figure 3. The ¹H NMR spectrum of ractopamine HCl in d₆DMSO.

Monte Carlo simulated annealing techniques as implemented in DASH (David et al., 2006), with the S,S cation and a Cl atom as fragments.

The neutral molecule was protonated at the N atom, and converted to the S,R configuration using Materials Studio (Dassault Systèmes, 2022). The structure was solved independently using this cation and a Cl atom with EXPO2014 (Altomare et al., 2013).

NMR analysis of ractopamine HCl was performed using a 400-MHz Bruker Avance spectrometer equipped with a multinuclear probe with the pharmaceutical in d₆DMSO (d₆DMSO was stored over flame dried 3 Å molecular sieves). As shown in Figure 3, the proton NMR spectra indicated that the molecule was protonated at the secondary amine of ractopamine. Interestingly, one of the resonances assigned to the N–H proton is the result of two closely overlapping broad singlets, which are likely the result of the two sets of diastereomers present in the sample.

Rietveld refinements of both structures (S,S and S,R) were carried out using GSAS-II (Toby and Von Dreele, 2013). A third refinement, with a 50/50 mixture of S,S and R,S molecules, yielded much higher residuals ($R_{wp} \sim 0.14$) and will not be discussed further. Only the 1.0°–25.0° (S,S) and 1.0°–22.0° (S,R) portions of the diffraction patterns were included in the refinements ($d_{\min} = 1.058$ and 1.201 Å, respectively). All non-H bond distances and angles were subjected to restraints, based on a Mercury/Mogul Geometry check (Bruno et al., 2004; Sykes et al., 2011). The Mogul average and

standard deviation for each quantity were used as the restraint parameters. Planar restraints were also applied to the phenyl rings. The restraints contributed 6.9 and 3.6% to the final χ^2 . The hydrogen atoms were included in calculated positions, which were recalculated during the refinement using Materials Studio (Dassault Systèmes, 2022). The U_{iso} of the heavy atoms were grouped by chemical similarity. The U_{iso} for the H atoms were fixed at 1.3× the U_{iso} of the heavy atoms to which they are attached. A fourth-order spherical harmonics model for preferred orientation was included in the refinements; the refined texture indices were 1.289 and 1.297. The peak profiles were described using the generalized microstrain model (Stephens, 1999). The background was modeled using

TABLE I. Refinement residuals for ractopamine hydrochloride

Model	S,S	S,R
# of variables	97	97
# of observations	23,408	20,516
# of restraints	55	55
R_{wp}	0.0954	0.0990
GOF	1.73	1.82
ΔF , +, eÅ ⁻³	1.45(12)	0.46(9)
	at Cl	at Cl
ΔF , -, eÅ ⁻³	-0.44(12)	-0.30(9)
		0.49 Å from C19
VASP energy, eV/cell	-27,263.908	-27,293.691
ΔE , kcal/mol	85.8	0

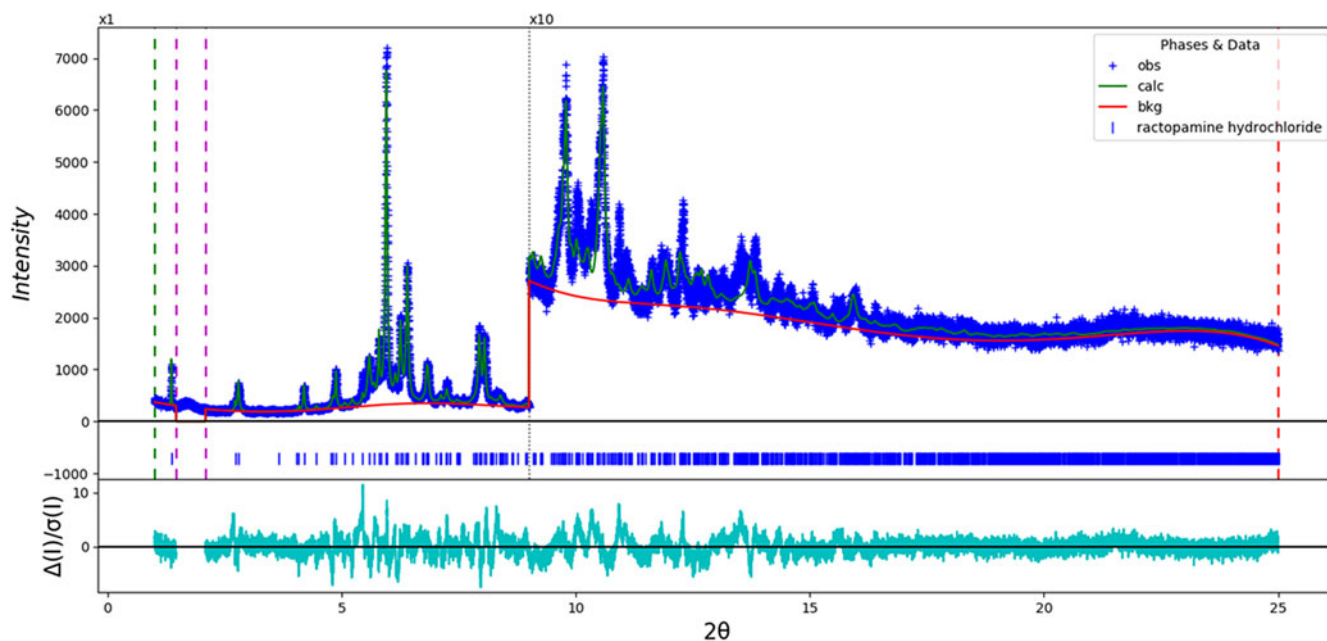


Figure 4. The Rietveld plot for the refinement of S,S-ractopamine hydrochloride. The blue crosses represent the observed data points, and the green line is the calculated pattern. The cyan curve is the normalized error plot, and the red line is the background curve. The vertical scale has been multiplied by a factor of 10× for $2\theta > 9.0^\circ$.

a six-term shifted Chebyshev polynomial, and a peak at 6.50° 2θ to model the scattering from the Kapton capillary and any amorphous component.

The final refinements yielded the residuals reported in Table I. The largest errors in the final difference plots (Figures 4 and 5) are small, and reflect fitting ordered models to a disordered system.

The structures of S,S and S,R ractopamine hydrochloride were optimized (fixed experimental unit cell) with density functional theory techniques using VASP (Kresse and

Furthmüller, 1996) through the MedeA graphical interface (Materials Design, 2016). The calculations were carried out on 16 2.4 GHz processors (each with 4-Gb RAM) of a 64-processor HP Proliant DL580 Generation 7 Linux cluster at North Central College. The calculations used the GGA-PBE functional, a plane wave cutoff energy of 400.0 eV, and a k -point spacing of 0.5 \AA^{-1} leading to a $1 \times 2 \times 2$ mesh, and took ~ 35 (S,S) and 48 (S,R) days. Rietveld refinements using the fixed VASP-optimized structures yielded much higher residuals, with R_{wp} around 32%. Single-point density

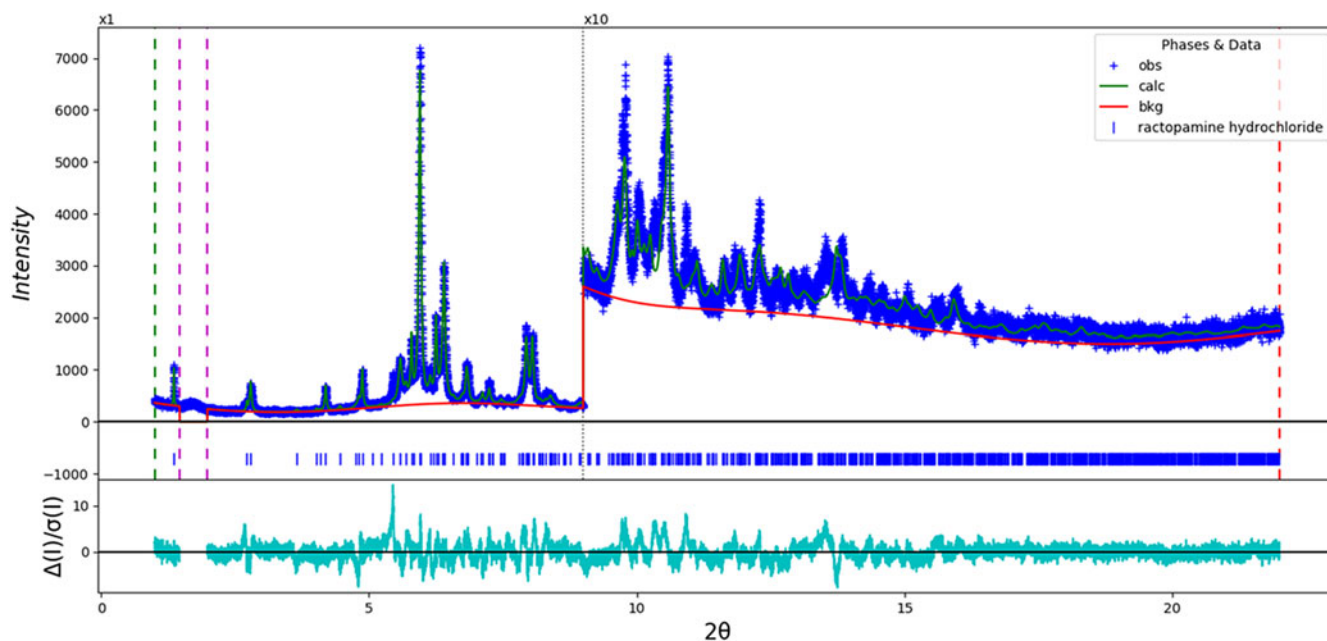


Figure 5. The Rietveld plot for the refinement of S,R-ractopamine hydrochloride. The blue crosses represent the observed data points, and the green line is the calculated pattern. The cyan curve is the normalized error plot, and the red line is the background curve. The vertical scale has been multiplied by a factor of 10× for $2\theta > 9.0^\circ$.

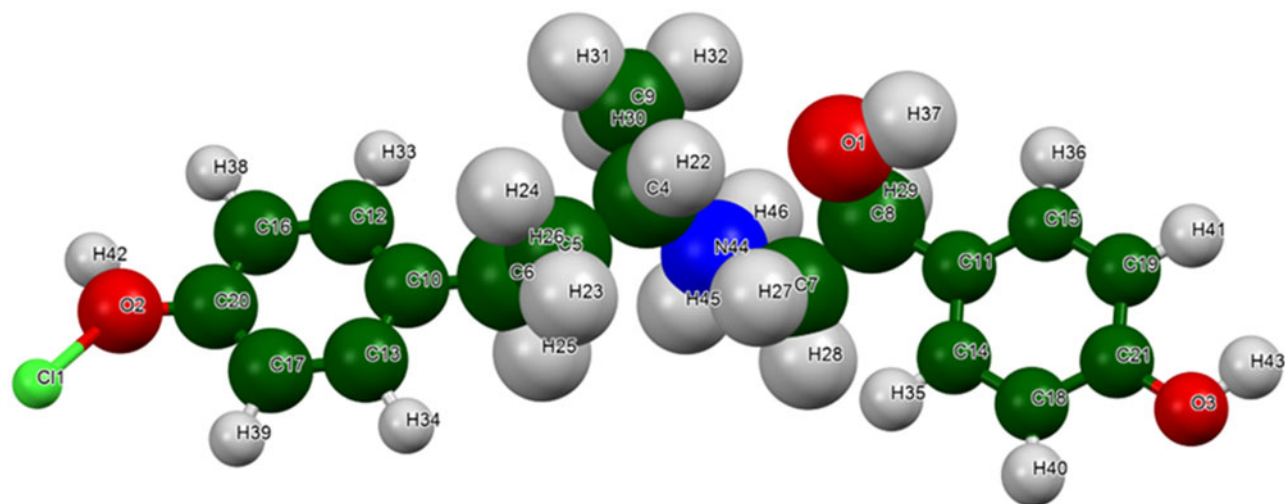


Figure 6. The asymmetric unit of S,S-ractopamine hydrochloride, with the atom numbering. The atoms are represented by 50% probability spheroids. Image generated using Mercury (Macrae et al., 2020).

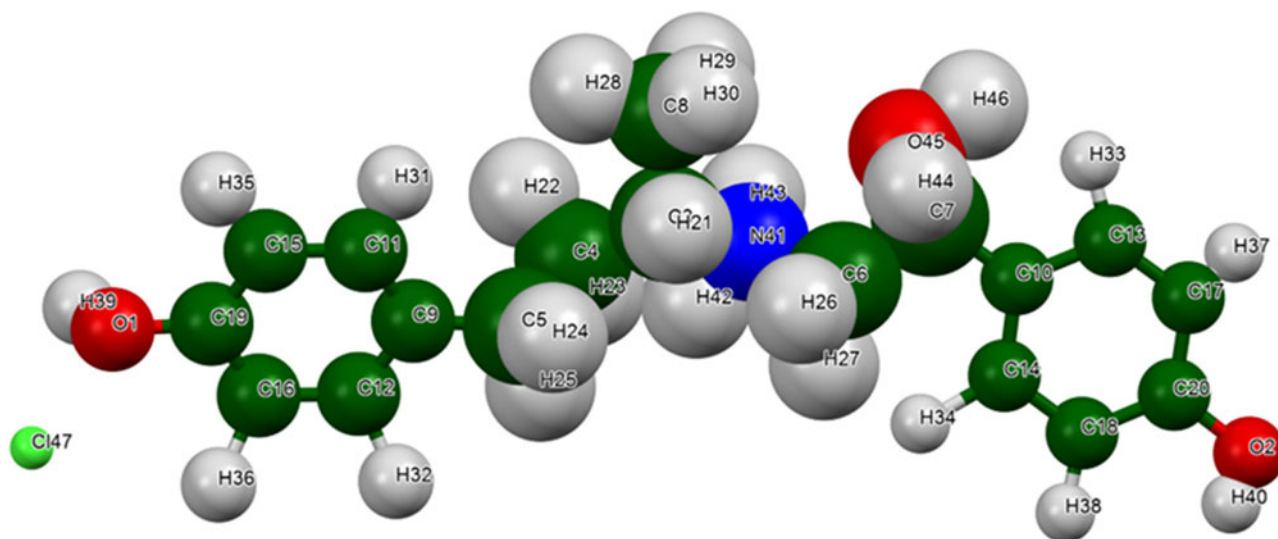


Figure 7. The asymmetric unit of S,R-ractopamine hydrochloride, with the atom numbering. The atoms are represented by 50% probability spheroids. Image generated using Mercury (Macrae et al., 2020).

functional theory calculations (fixed experimental cell) and population analysis were carried out using CRYSTAL23 (Erba et al., 2023). The basis sets for the H, C, N, and O atoms in the calculation were those of Gatti et al. (1994), and that for Cl was that of Peintinger et al. (2013). The calculations were run on a 3.5 GHz PC using eight k -points and the B3LYP functional, and took ~ 3.4 (S,S) and 3.5 (S,R) hr.

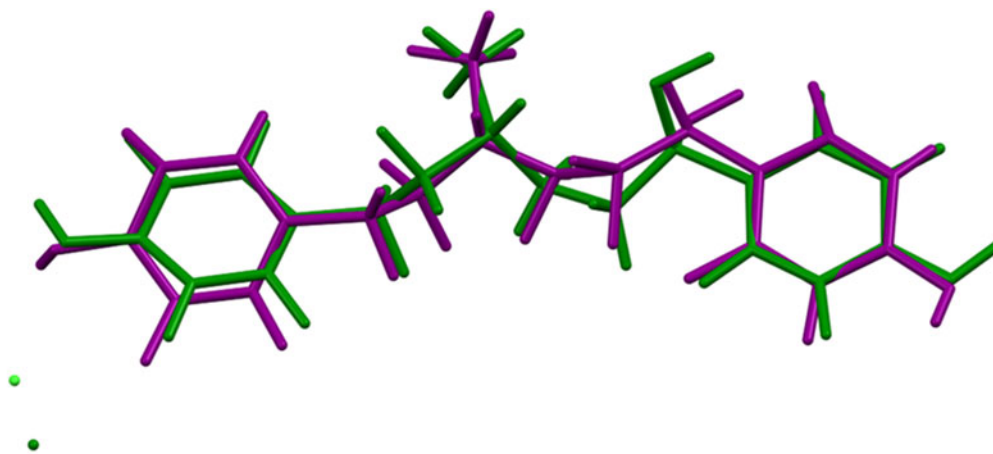
III. RESULTS AND DISCUSSION

Two different ordered models (S,S and S,R) for ractopamine hydrochloride have been refined, for a sample which consists of a mixture of S,S/R,R/S,R and R,S forms. Powder diffraction cannot distinguish the two racemic pairs, so refinement of two diastereomers was sufficient. In *Pbca*, each structural model contains both members of an enantiomeric pair. The asymmetric units (with atom numbering) are illustrated in Figures 6 and 7. The displacement coefficients in the centers of the molecules are large, reflecting the disorder.

Refinements of the two models yielded comparable residuals, but the S,R model is significantly lower in energy. The S,S model also resulted in an unreasonably short cation-anion distance. The S,R model is thus to be preferred for this disordered system.

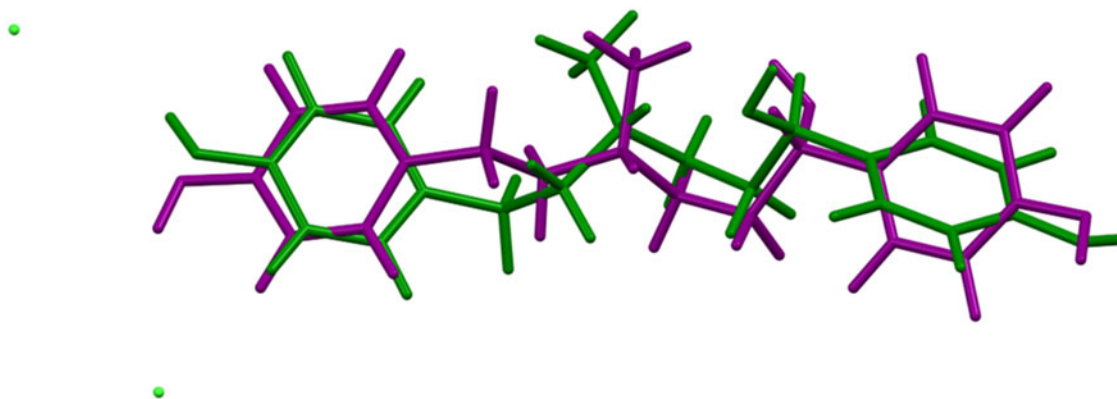
The root-mean-square (rms) Cartesian displacement of the refined S,S and S,R molecules is 0.770 Å (Figure 8). The rms displacement for the VASP-optimized molecules is 1.079 Å (Figure 9). The overall shapes of the molecules are similar, making it non-unreasonable that they could be accommodated in the same lattice. The average microstrains for the two models are 17,479 (S,S) and 16,917 (S,R) ppm, reflecting the imperfect nature of the crystals.

The rms displacement between the Rietveld-refined and VASP-optimized S,S cations is 0.637 Å (Figure 10), and the displacement between the S,R cations is 0.668 Å (Figure 11). The agreements are outside the normal range for correct structures (van de Streek and Neumann, 2014), but this is to be expected from refining ordered models of a



Experimental: g = green, h = purple; rmscd = 0.770, inverted = 0.421

Figure 8. Comparison of the as-refined S,S (green) and S,R (purple) ractopamine cations. The rms deviation is 0.770 Å native, and 0.421 Å inverted. Image generated using Mercury (Macrae et al., 2020).



VASP; g = green, h = purple; rmscd = 1.079, inverted = 0.900

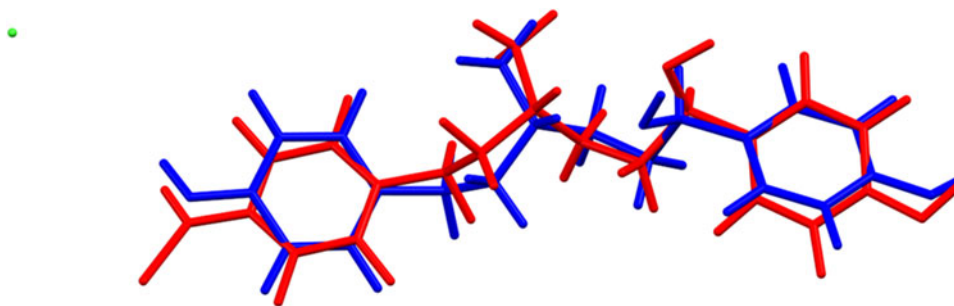
Figure 9. Comparison of the VASP-optimized S,S (green) and S,R (purple) ractopamine cations. The rms deviation is 1.079 Å native, and 0.900 Å inverted. Image generated using Mercury (Macrae et al., 2020).

disordered structure. Overlays of the refined and optimized structures of the S,S and S,R models are presented in Figures 12 and 13. A more-standard picture of the optimized S,R structure is included as Figure 14. The remaining discussion will concentrate on the VASP-optimized structures.

The crystal structure consists of layers of molecules parallel to the *bc*-plane (Figure 14). The mean planes of the phenyl rings in the S,S molecule are (5,2,7) and (7,8,7), while those in the S,R molecule are (1,1,-1) and (-5,-3,4); the orientations of the rings thus differ in the two structures. The Mercury Aromatics Analyser indicates only weak interactions (>4.9 Å) in the two structures. N-H...Cl hydrogen bonds link the cations and anions.

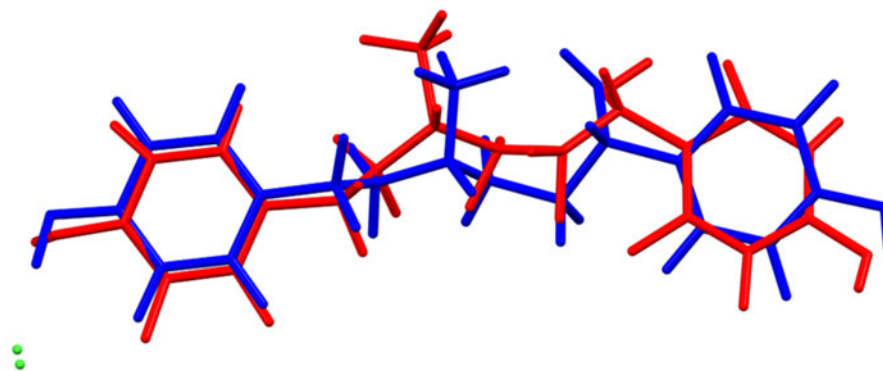
Almost all of the bond distances and bond angles fall within the normal ranges indicated by a Mercury Mogul Geometry check (Macrae et al., 2020). Only the C6-C5-C4 angle of 117.8° (average = 113.6(14)°; Z-score = 3.0) in the S,S molecule is flagged as unusual. Torsion angles in S,S involving rotation about the C4-N44 and C5-C6 bonds lie in minor populations of trimodal *gauche/trans* distributions, and are flagged as unusual. Torsion angles involving rotation about the C7-C10 bond are approximately 0/180°, on the tails of a broad distribution centered about 90°.

Quantum chemical geometry optimizations of the isolated cations (DFT/B3LYP/6-31G*/water) using Spartan '18 (Wavefunction, 2020) indicated that the S,R cation is



G (S,S): rmscd = 0.637

Figure 10. Comparison of the Rietveld-refined (red) and VASP-optimized (blue) structures of the S,S-ractopamine cation. The rms Cartesian displacement is 0.637 Å. Image generated using Mercury (Macrae et al., 2020).



H; rmscd = 0.668

Figure 11. Comparison of the Rietveld-refined (red) and VASP-optimized (blue) structures of the S,R-ractopamine cation. The rms Cartesian displacement is 0.668 Å. Image generated using Mercury (Macrae et al., 2020).

1.2 kcal/mol lower in energy than the S,S cation, but this difference lies within the expected error range of such calculations, so the two molecules should be considered equivalent in energy. The global minimum-energy conformations (MMFF force field) of both the S,S and S,R cations are much more compact (fold on themselves), showing that intermolecular interactions are important in determining the observed solid-state conformations.

Analysis of the contributions to the total crystal energy of the structure using the Forcite module of Materials Studio (Dassault Systèmes, 2022) suggests that bond, angle, and torsion distortion terms dominate the intramolecular deformation energy. The intermolecular energy is dominated by electrostatic attractions, which in this force field analysis also include hydrogen bonds. The hydrogen bonds are better analyzed using the results of the DFT calculation.

Hydrogen bonds are prominent in both the S,S and S,R structures (Tables II and III). As expected, in each structure

one of the H atoms on the protonated N atom acts as a donor in a strong discrete N–H⋯Cl hydrogen bond. In the S,R structure this H also forms a weak intramolecular N–H⋯O hydrogen bond, and the other H atom on the N also forms an intramolecular N–H⋯O hydrogen bond. In each structure, hydroxyl groups act as donors in O–H⋯Cl and O–H⋯O hydrogen bonds. The energies of the O–H⋯Cl hydrogen bonds were calculated using the correlation of Rammohan and Kaduk (2018), the energies of the N–H⋯O hydrogen bonds were calculated using the correlation of Wheatley and Kaduk (2019), and the energies of the O–H⋯Cl hydrogen bonds were calculated using a correlation implicit in Kaduk (2002). In the S,S structure the classical hydrogen bonds link the molecules into chains parallel to the *a*-axis, while in the S,R structure, they link the molecules into corrugated chains parallel to the *b*-axis. There are several C–H⋯Cl and C–H⋯O hydrogen bonds, which vary between the two structures.

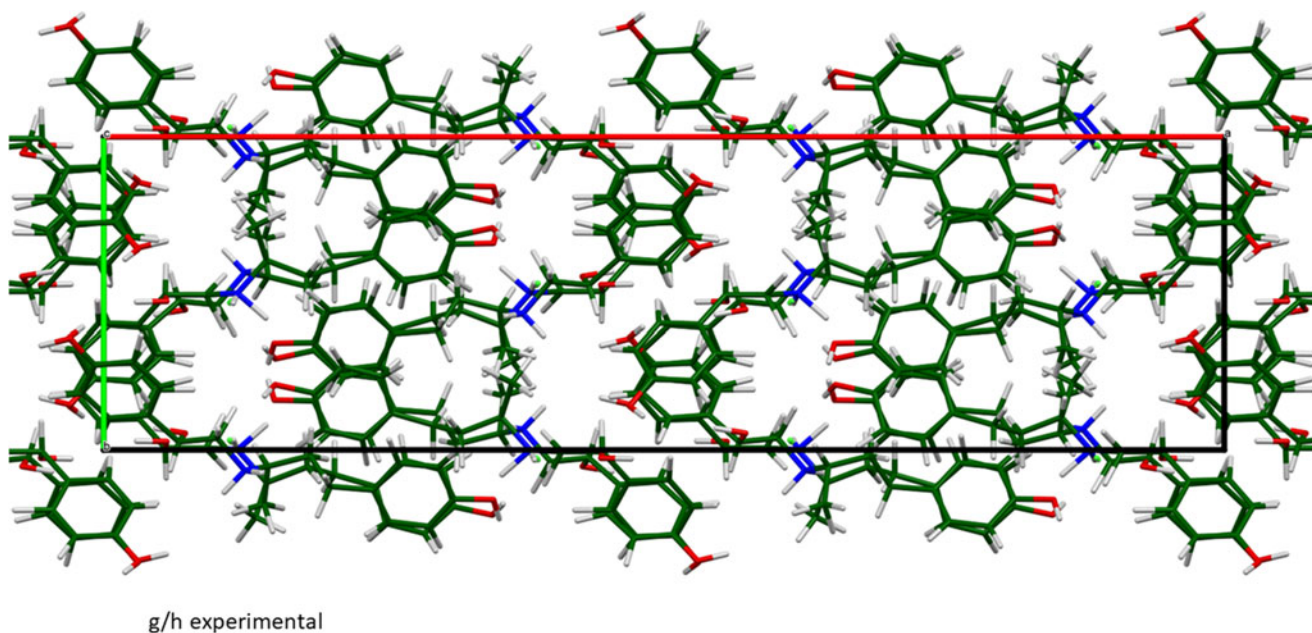


Figure 12. Overlap of the refined S,S, and S,R structures of ractopamine hydrochloride, viewed down the *c*-axis. Image generated using Mercury (Macrae et al., 2020).

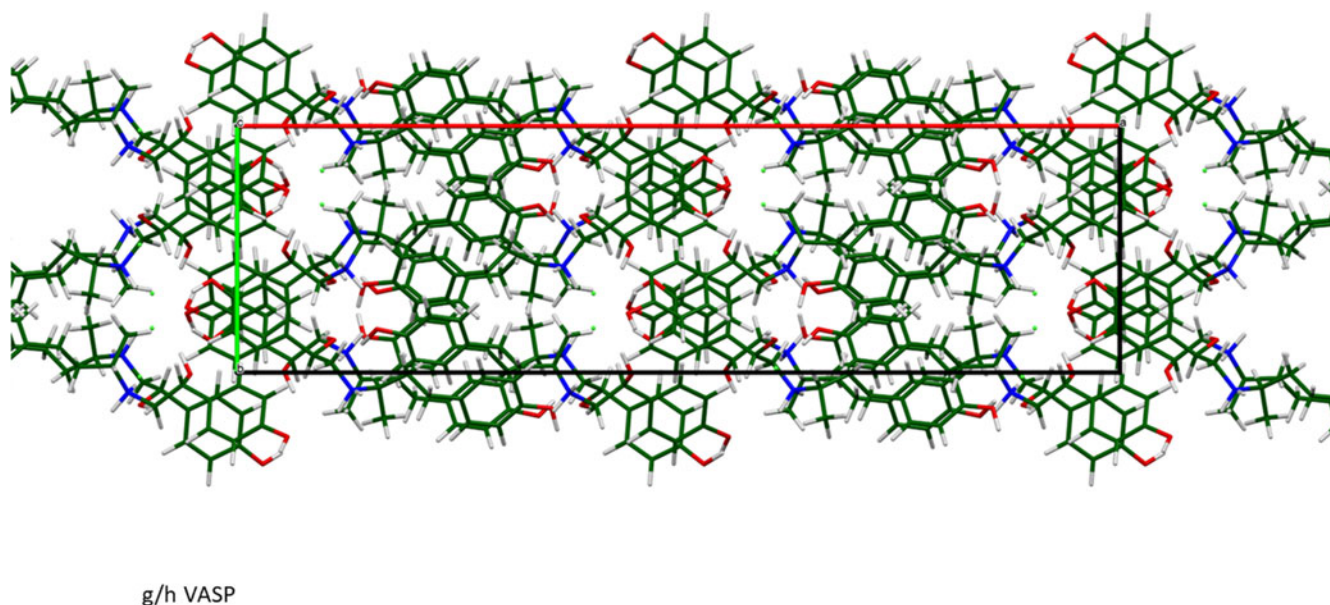


Figure 13. Overlap of the VASP-optimized S,S, and S,R structures of ractopamine hydrochloride, viewed down the *c*-axis. Image generated using Mercury (Macrae et al., 2020).

The volumes enclosed by the Hirshfeld surface of the ractopamine hydrochloride asymmetric unit (Figures 15 and 16, Hirshfeld, 1977; Spackman et al., 2021) are 428.59 and 428.02 Å³, 98.1 and 98.2% of the unit cell volume. The packing density is thus fairly typical. The only significant close contacts (red in Figures 15 and 16) involve the hydrogen bonds. The volume/non-hydrogen atom is larger than normal, at 19.0 Å³, reflecting the presence of the large chloride anion.

The Bravais–Friedel–Donnay–Harker (Bravais, 1866; Friedel, 1907; Donnay and Harker, 1937) morphology suggests that we might expect platy morphology for ractopamine hydrochloride, with {100} as the major faces. A fourth-order

spherical harmonics model for preferred orientation was included in the refinements; the refined texture indices were 1.289 and 1.297, indicating that preferred orientation was significant in this rotated capillary specimen.

IV. DEPOSITED DATA

The powder pattern of ractopamine hydrochloride from this synchrotron data set has been submitted to ICDD for inclusion in the Powder Diffraction File. The Crystallographic Information Framework (CIF) files containing the results of the Rietveld refinement (including the raw

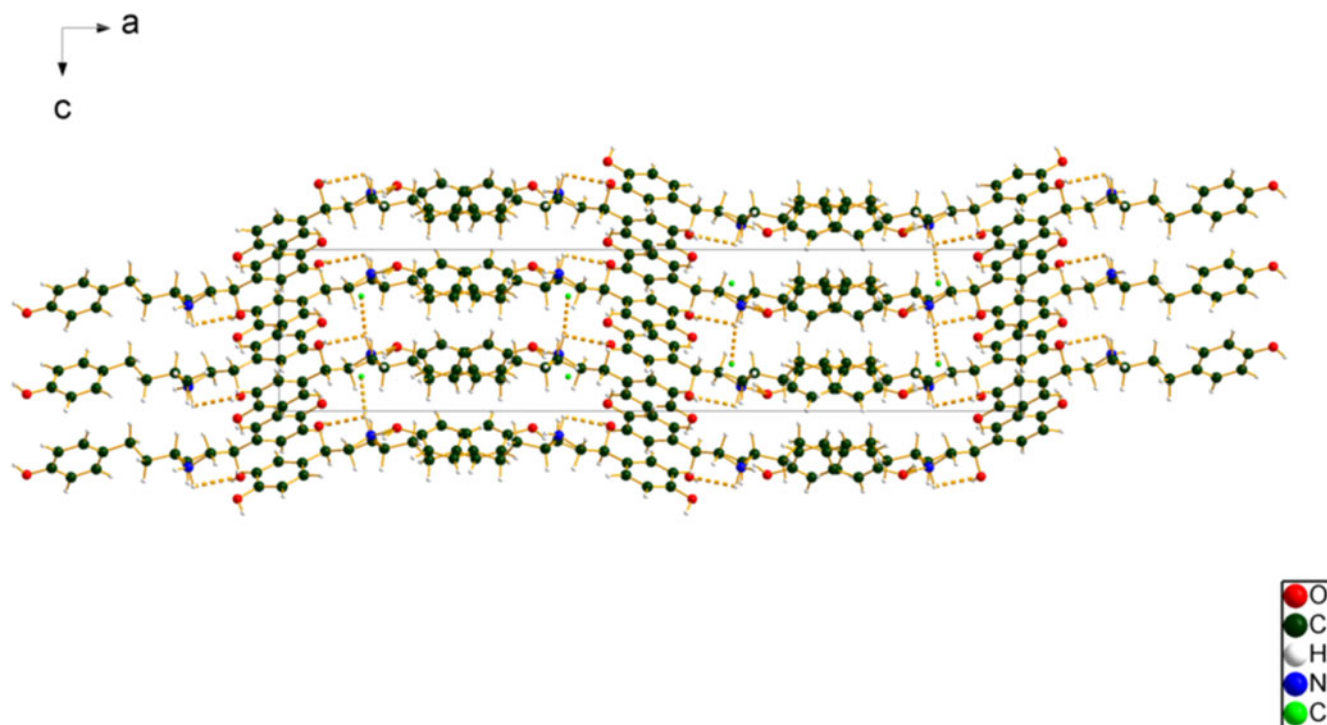


Figure 14. The crystal structure of ractopamine hydrochloride, viewed down the *b*-axis. Image generated using Diamond (Crystal Impact, 2022).

TABLE II. Hydrogen bonds (CRYSTAL23) in S,S-ractopamine hydrochloride

H-bond	D-H, Å	H...A, Å	D...A, Å	D-H...A, °	Overlap, <i>e</i>	<i>E</i> , kcal/mol
N41–H43...Cl47	1.096	1.917	2.996	167.4	0.133	
O2–H40...Cl47	0.998	2.115	3.039	153.2	0.070	37.2
O1–H39...O45	0.994	1.857	2.811	159.7	0.059	13.3
O45–H46...C14	0.981	2.585	3.547	167.0	0.015	
C17–H37...O2	1.090	2.346	3.321	148.0	0.023	
C16–H36...Cl47	1.093	3.152	4.175	156.1	0.018	
C13–H33...O1	1.093	2.424	3.470	159.7	0.019	
C8–H30...Cl47	1.099	2.862	3.892	156.1	0.028	
C7–H44...O2	1.105	2.598	3.584	148.1	0.015	
C6–H26...O1	1.098	2.504	3.231	122.6	0.011	
C3–H21...O45	1.097	2.132 ^a	3.065	141.3	0.024	

^aIntramolecular charge.

TABLE III. Hydrogen bonds (CRYSTAL23) in S,R-ractopamine hydrochloride

H-bond	D-H, Å	H...A, Å	D...A, Å	D-H...A, °	Overlap, <i>e</i>	<i>E</i> , kcal/mol
N41–H43...Cl47	1.067	2.100	3.155	169.7	0.098	
N41–H43...O5	1.067	2.536 ^a	2.868	96.9	0.013	2.6
N41–H42...O1	1.046	1.969	2.973	169.6	0.059	5.6
O2–H40...O45	0.984	2.391	2.888	86.8	0.022	8.1
O1–H39...Cl47	1.020	1.945	2.964	176.9	0.097	43.8
O45–H46...O2	0.980	2.038	2.888	144.0	0.040	10.9
C18–H38...O45	1.087	2.338	3.171	132.1	0.014	
C17–H37...Cl47	1.093	2.643	3.630	149.9	0.034	
C8–H29...Cl47	1.100	2.972	3.829	135.0	0.014	
C16–H36...Cl47	1.042	2.720	3.529	130.6	0.025	
C8–H30...O2	1.096	2.660	3.660	151.6	0.011	

^aIntramolecular charge.

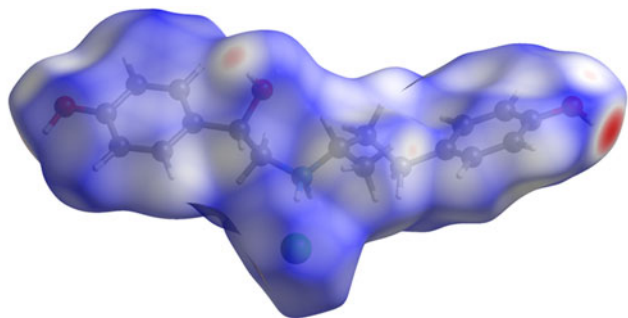


Figure 15. The Hirshfeld surface of S,S-ractopamine hydrochloride. Intermolecular contacts longer than the sums of the van der Waals radii are colored blue, and contacts shorter than the sums of the radii are colored red. Contacts equal to the sums of radii are white. Image generated using CrystalExplorer (Spackman et al., 2021).

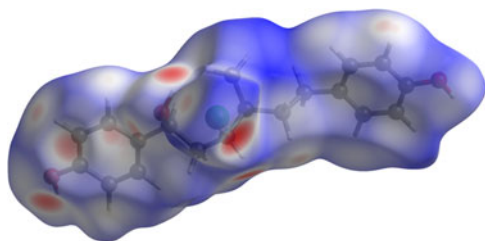


Figure 16. The Hirshfeld surface of S,R-ractopamine hydrochloride. Intermolecular contacts longer than the sums of the van der Waals radii are colored blue, and contacts shorter than the sums of the radii are colored red. Contacts equal to the sums of radii are white. Image generated using CrystalExplorer (Spackman et al., 2021).

data) and the DFT geometry optimization were deposited with the ICDD. The data can be requested at pdj@icdd.com.

ACKNOWLEDGEMENTS

Use of the Advanced Photon Source at Argonne National Laboratory was supported by the U.S. Department of Energy, Office of Science, Office of Basic Energy Sciences, under Contract No. DE-AC02-06CH11357. This work was partially supported by the International Centre for Diffraction Data. We thank Lynn Ribaud and Saul Lapidus for their assistance in the data collection.

CONFLICTS OF INTEREST

The authors have no conflicts of interest to declare.

REFERENCES

- Altomare, A., C. Cuocci, C. Giacovazzo, A. Moliterni, R. Rizzi, N. Corriero, and A. Falcicchio. 2013. "EXPO2013: A Kit of Tools for Phasing Crystal Structures from Powder Data." *Journal of Applied Crystallography* 46: 1231–35.
- Antao, S. M., I. Hassan, J. Wang, P. L. Lee, and B. H. Toby. 2008. "State-of-the-Art High-Resolution Powder X-Ray Diffraction (HRPXRD) Illustrated with Rietveld Refinement of Quartz, Sodalite, Tremolite, and Meionite." *Canadian Mineralogist* 46: 1501–9.
- Bravais, A. 1866. *Etudes Cristallographiques*. Paris, Gauthier Villars.
- Bruno, I. J., J. C. Cole, M. Kessler, J. Luo, W. D. S. Motherwell, L. H. Purkis, B. R. Smith, R. Taylor, R. I. Cooper, S. E. Harris, and A. G. Orpen. 2004.

- "Retrieval of Crystallographically-Derived Molecular Geometry Information." *Journal of Chemical Information and Computer Sciences* 44: 2133–44.
- Crystal Impact. 2022. Diamond. V. 4.6.8. Crystal Impact - Dr. H. Putz & Dr. K. Brandenburg. Windows.
- Dassault Systèmes. 2022. *Materials Studio 2023*. San Diego, CA, BIOVIA.
- David, W. I. F., K. Shankland, J. van de Streek, E. Pidcock, W. D. S. Motherwell, and J. C. Cole. 2006. "DASH: A Program for Crystal Structure Determination from Powder Diffraction Data." *Journal of Applied Crystallography* 39: 910–5.
- Donnay, J. D. H., and D. Harker. 1937. "A New Law of Crystal Morphology Extending the Law of Bravais." *American Mineralogist* 22: 446–66.
- Erba, A., J. K. Desmaris, S. Casassa, B. Civalleri, L. Donà, I. J. Bush, B. Searle, L. Maschio, L.-E. Daga, A. Cossard, C. Ribaldone, E. Ascricchi, N. L. Marana, J.-P. Flament, and B. Kirtman. 2023. "CRYSTAL23: A Program for Computational Solid State Physics and Chemistry." *Journal of Chemical Theory and Computation* 19: 6891–932. doi:10.1021/acs.jctc.2c00958.
- Friedel, G. 1907. "Etudes sur la loi de Bravais." *Bulletin de la Société Française de Minéralogie* 30: 326–455.
- Gates-Rector, S., and T. N. Blanton. 2019. "The Powder Diffraction File: A Quality Materials Characterization Database." *Powder Diffraction* 39: 352–60.
- Gatti, C., V. R. Saunders, and C. Roetti. 1994. "Crystal-Field Effects on the Topological Properties of the Electron-Density in Molecular Crystals - the Case of Urea." *Journal of Chemical Physics* 101: 10686–96.
- Groom, C. R., I. J. Bruno, M. P. Lightfoot, and S. C. Ward. 2016. "The Cambridge Structural Database." *Acta Crystallographica Section B: Structural Science, Crystal Engineering and Materials* 72: 171–9.
- Gunnar, A. K., K. Reuter, V. Meier, & E. Gogritchiani. 2009. Use of RR/SR-Ractopamine. U.S. Patent Application 2009/0143480 A1.
- Hirshfeld, F. L. 1977. "Bonded-Atom Fragments for Describing Molecular Charge Densities." *Theoretica Chimica Acta* 44: 129–38.
- Kaduk, J. A. 2002. "Use of the Inorganic Crystal Structure Database as a Problem Solving Tool." *Acta Crystallographica B* 58: 370–9.
- Kaduk, J. A., C. E. Crowder, K. Zhong, T. G. Fawcett, and M. R. Suchomel. 2014. "Crystal Structure of Atomoxetine Hydrochloride (Strattera), C₁₇H₂₂NOCl." *Powder Diffraction* 29: 269–73.
- Kim, S., J. Chen, T. Cheng, A. Gindulyte, J. He, S. He, Q. Li, B. A. Shoemaker, P. A. Thiessen, B. Yu, L. Zaslavsky, J. Zhang, and E. E. Bolton. 2023. "Pubchem 2023 Update." *Nucleic Acids Research* 51 (D1): D1373–80. doi:10.1093/nar/gkac956.
- Kresse, G., and J. Furthmüller. 1996. "Efficiency of Ab-Initio Total Energy Calculations for Metals and Semiconductors Using a Plane-Wave Basis Set." *Computational Materials Science* 6: 15–50.
- Lee, P. L., D. Shu, M. Ramanathan, C. Preissner, J. Wang, M. A. Beno, R. B. Von Dreele, L. Ribaud, C. Kurtz, S. M. Antao, X. Jiao, and B. H. Toby. 2008. "A Twelve-Analyzer Detector System for High-Resolution Powder Diffraction." *Journal of Synchrotron Radiation* 15: 427–32.
- Louër, D., and A. Boulfif. 2007. "Powder Pattern Indexing and the Dichotomy Algorithm." *Zeitschrift für Kristallographie Supplementa* 26: 191.
- Macrae, C. F., I. Sovago, S. J. Cottrell, P. T. A. Galek, P. McCabe, E. Pidcock, M. Platings, G. P. Shields, J. S. Stevens, M. Towler, and P. A. Wood. 2020. "Mercury 4.0: From Visualization to Design and Prediction." *Journal of Applied Crystallography* 53: 226–35.
- Materials Design. 2016. *MedeA 2.20.4*. Angel Fire, NM, Materials Design Inc.
- MDI. 2023. *JADE Pro version 8.8*. Livermore, CA, Materials Data.
- Mills, S. E., J. Kissel, C. A. Bidwell, and D. J. Smith. 2003a. "Stereoselectivity of Porcine β -Adrenergic for Ractopamine Stereoisomers." *Journal of Animal Science* 81: 122–9.
- Mills, S. E., M. E. Spurlock, and D. J. Smith. 2003b. " β -Adrenergic Receptor Subtypes that Mediate Ractopamine Stimulation of Lypolysis." *Journal of Animal Science* 81: 662–8.
- O'Boyle, N. M., M. Banck, C. A. James, C. Morley, T. Vandermeersch, and G. R. Hutchison. 2011. "Open Babel: An Open Chemical Toolbox." *Journal of Chemical Informatics* 3: 33. doi:10.1186/1758-2946-3-33.
- Pacelle, W. 2014. "Banned in 160 Nations, Why is Ractopamine in U.S. Pork? (Op-Ed)." *Live Science*. Expert Voices: Op-Ed & Insights. <https://www.livescience.com/47032-time-for-us-to-ban-ractopamine.html>
- Peintinger, M. F., D. Vilela Oliveira, and T. Bredow. 2013. "Consistent Gaussian Basis Sets of Triple-Zeta Valence with Polarization quality for

- Solid-State Calculations.” *Journal of Computational Chemistry* 34: 451–9.
- Petricek, V., M. Dusek, and L. Palatinus. 2014. “Crystallographic Computing System JANA2006: General features.” *Zeitschrift für Kristallographie-Crystalline Materials* 229: 345–52.
- Rammohan, A., and J. A. Kaduk. 2018. “Crystal Structures of Alkali Metal (Group 1) Citrate Salts.” *Acta Crystallographica Section B: Crystal Engineering and Materials* 74: 239–52. doi:10.1107/S2052520618002330.
- Ricke, E. A., D. J. Smith, V. J. Feil, G. L. Larsen, and J. S. Caton. 1999. “Effects of Ractopamine HCl Stereoisomers on Groth, Nitrogen Retention, and Carcass Composition in Rats.” *Journal of Animal Science* 77: 701–7.
- Spackman, P. R., M. J. Turner, J. J. McKinnon, S. K. Wolff, D. J. Grimwood, D. Jayatilaka, and M. A. Spackman. 2021. “Crystalexplorer: A Program for Hirshfeld Surface Analysis, Visualization and Quantitative Analysis of Molecular Crystals.” *Journal of Applied Crystallography* 54: 1006–11. doi:10.1107/S1600576721002910.
- Stephens, P. W. 1999. “Phenomenological Model of Anisotropic Peak Broadening in Powder Diffraction.” *Journal of Applied Crystallography* 32: 281–9.
- Sykes, R. A., P. McCabe, F. H. Allen, G. M. Battle, I. J. Bruno, and P. A. Wood. 2011. “New Software for Statistical Analysis of Cambridge Structural Database Data.” *Journal of Applied Crystallography* 44: 882–6.
- Toby, B. H., and R. B. Von Dreele. 2013. “GSAS II: The Genesis of a Modern Open Source All Purpose Crystallography Software Package.” *Journal of Applied Crystallography* 46: 544–9.
- van de Streek, J., and M. A. Neumann. 2014. “Validation of Molecular Crystal Structures from Powder Diffraction Data with Dispersion-Corrected Density Functional Theory (DFT-D).” *Acta Crystallographica Section B: Structural Science, Crystal Engineering and Materials* 70: 1020–32.
- Wang, J., B. H. Toby, P. L. Lee, L. Ribaud, S. M. Antao, C. Kurtz, M. Ramanathan, R. B. Von Dreele, and M. A. Beno. 2008. “A Dedicated Powder Diffraction Beamline at the Advanced Photon Source: Commissioning and Early Operational Results.” *Review of Scientific Instruments* 79: 085105.
- Wavefunction, Inc. 2020. Spartan ‘18. Version 1.4.5. Wavefunction Inc., 18401 Von Karman Ave., Suite 370, Irvine CA 96212.
- Wheatley, A. M., and J. A. Kaduk. 2019. “Crystal Structures of Ammonium Citrates.” *Powder Diffraction* 34: 35–43.